JOURNAL OF THERMOPHYSICS AND HEAT TRANSFER
Vol. 18, No. 3, July–September 2004

Nonequilibrium Phenomena Behind Strong Shock Waves Generated in Superorbital Reentry Flight

Atsushi Matsuda*
University of Tokyo, Tokyo 113-8654, Japan
and
Kazuhisa Fujita,† Shunichi Sato,‡ and Takashi Abe§
Institute of Space and Astronautical Science, Kanagawa 229-8510, Japan

The aerothermodynamic behavior behind the strong shock wave in air that is associated with a superorbital reentry flight was investigated experimentally. For the experiment, a free-piston-driven shock tube was used, and radiation from behind the shock front was investigated spectroscopically. Based on the spectroscopic measurement, the spatial distributions of the rotational/vibrational temperatures of molecules (N_2 and N_2^+), the electron excitation temperature of atomic nitrogen N, and the electron density were determined in the region behind the shock front. These results were reviewed by comparison with those previously determined for a nitrogen gas. It was found that there is remarkable resemblance in such distributions between air and a nitrogen gas. This suggests that the existence of molecular oxygen in air has only a minor influence on the behavior of temperatures of N_2, N_2^+, and N, and of the electron density.

I. Introduction

A SAMPLE return mission called the MUSES-C program has been in progress at the Institute of Space and Astronautical Science in Japan.[1] This program's mission is to bring back a sample of an asteroid's soil to Earth. One of the highlighted technologies in the program is the direct reentry to the Earth atmosphere from interplanetary orbit, with a reentry velocity as high as 12 km/s. For such a reentering capsule, the development of the thermal protection system is one of the most challenging technical issues because the aerothermodynamic flight environment in such a high-velocity reentry is expected to be very severe with regard to aerodynamic heating. Thus, for the development of such a vehicle, the extent of aerodynamic heating must be predicted. Note, however, that the nonequilibrium behavior of the shock layer plays an important role, and, therefore, extensive work on nonequilibrium behavior has already been carried out. Still, the nonequilibrium behavior of the shock layer at high-speed reentry, is not yet fully understood.

Previously, the strong shock wave corresponding to a superorbital reentry velocity in a nitrogen gas, has been investigated. In the experiment, it was found that various nonequilibrium behaviors, most of which show disagreement with the prediction based on the conventional aerothermochemical model,[2,3] do exist. For the design of a capsule reentering the Earth atmosphere, however, knowledge of the strong shock wave in air is required. Although the investigation on the strong shock wave in a nitrogen gas gives us valuable information, the information is indirect, and direct information is desired. In this paper, we attempt to investigate the strong shock wave in air. As a first step of the investigation, we focus on nitrogen-originated species such as N_2, N_2^+, N, and electrons that were fully investigated previously for a nitrogen gas, and we examine the effect of oxygen on the behavior of such species.

Presented as Paper 2002-3101 at the AIAA/ASME 8th Joint Thermophysics and Heat Transfer Conference, St. Louis, MO, 22–24 June 2002; received 4 November 2003; revision received 17 February 2004; accepted for publication 17 February 2004.

*Graduate School Student, Department of Aeronautics and Astronautics, Hongo 7-3-1, Bunkyoku; matsuda@gd.isas.jaxa.jp. Student Member AIAA.
†Research Associate, Research Division for Space Transportation, Yoshinodai 3-1-1, Sagamihara. Member AIAA.
‡Technical Staff, Research Division for Space Transportation, Yoshinodai 3-1-1, Sagamihara.
§Professor, Research Division for Space Transportation, Yoshinodai 3-1-1, Sagamihara; also Professor, University of Tokyo. Associate Fellow AIAA.

II. Experimental Setup

The present experiment employed the double diaphragm free-piston-driven shock tube available at the Institute of Space and Astronautical Science in Japan. In this shock tube, a strong shock wave with a shock propagation velocity up to approximately 15 km/s, with an initial ambient pressure of 0.1 torr for air, could be attained in the test tube with a square cross section, 35 mm on a side. The details of the facility are described in Refs. 2–4. As for the test gas in the present experiment, a gas mixture composed of 22% oxygen and 78% nitrogen was employed instead of atmospheric air to avoid any impurity in the test gas inside the test tube. As for the pressure of the test gas in the test tube, pressures of 2.1 and 0.3 torr were selected, which correspond to the shock wave propagation velocity of 8 and 12 km/s, respectively, under the present operating conditions. Note that the shock wave propagation velocity of 8 and 12 km/s correspond to the reentry velocity from lower Earth orbit and to the direct reentry velocity from an interplanetary orbit, respectively. The pressures 2.1 and 0.3 torr correspond to the atmospheric pressure at the 45- and 75-km altitudes, respectively.

To investigate the aerothermodynamic behavior behind the shock wave, the radiation emitted from the shock-heated region was spectroscopically investigated. Figure 1 shows the optical setup at the measurement section of the test tube. The details of the optical setup are available in Refs. 2 and 3. For measurement purposes, it is assumed that the flow generated by the shock wave is uniform in the cross section of the test tube and varies only along the distance from the shock wave. Because the shock wave generated in the test tube is almost plain and perpendicular to the test tube wall, this assumption is reasonable, especially when we focus on the region near the centerline of the shock tube not far from the shock front. Under this assumption, we will focus only on the radiation emitted from the region along the centerline of the test tube. To investigate it, the radiation emitted from the central region of the test section is focused on the entrance slit of the spectrometer (ORIEL MS127i) by means of an ellipsoidal mirror and is decomposed into a spectrum. Because the shock wave propagates through the test section, the temporal variation of the radiation at the region reflects the spatial variation along the distance from the shock wave. The instantaneous spectrum image of the radiation after the shock wave passage was recorded by means of an image-intensified charge-coupled device (ICCD)

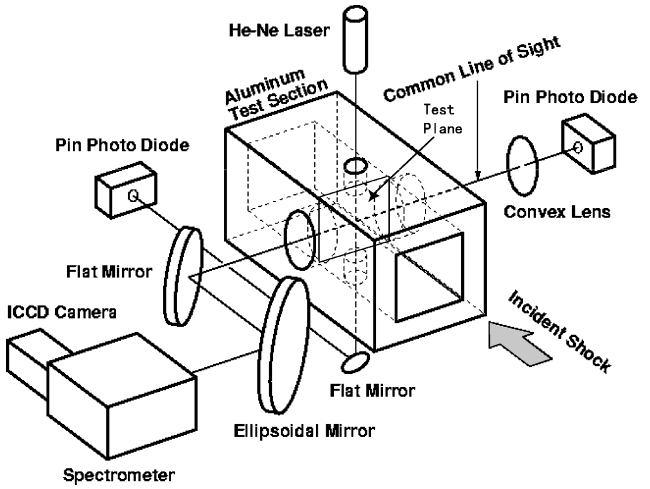

Fig. 1 Experimental setup of optical system.

camera (ANDOR IN-STA SPECV IS510), which was triggered by the signal delayed from the pressure sensor signal mounted upstream of the measurement section. In each run of the shock tube, one ICCD image of the radiation spectrum was recorded at a location with a specified distance away from the shock front. Accumulation of the radiation spectrum data for various locations was carried out by driving the ICCD camera with various delayed time intervals in repeated runs of the shock tube operation. The spatial resolution of the measurement in the present experiment depends on the gate time of the ICCD camera (100 ns), but can be kept to less than 1.2 mm. For this method to make sense, the reproducibility of each run of the shock tube is necessary. Even though the reproducibility of each run is fairly good, it is still desirable to discriminate between each run to secure exact reproducibility. For this purpose, the reproducibility of the flow at each run was monitored. Not only the temporal behavior of the pressure signals and the shock propagation velocity measured from the pressure signals were monitored, but so was the distribution of the total radiation intensity. Throughout the present experiment, the reproducibility remained reasonably good. To detect the shock front that gives an origin of the distance from the shock front, the laser schlieren technique was employed.

III. Radiation Spectrum

A. Spectrum in 12 km/s Case

The typical radiation spectrum in the case of a shock propagation velocity of 12.4 km/s is shown in Fig. 2, where the spectrum was recorded at a location 1.4 mm away from the shock front. As shown in Fig. 2, the wavelength range from 250 to 500 nm is mainly dominated by the molecular band of $N_2(2+)$ and $N_2^+(1-)$ whose behavior reflects the rotational and vibrational temperatures of N_2 and N_2^+, respectively. This means that those temperatures can be determined from the measured spectrum. The detailed procedure for the determination will be explained later. The emission observed at 485 nm is the Balmer line of atomic hydrogen that originates from the water vapor evaporated from the shock tube inner surface. The water vapor is expected to be caused by the inevitable exposure of the shock tube inner surface to the atmosphere, especially when the diaphragms in the shock tube are replaced. The Balmer line could be affected by various effects and varies its appearance, for instance, broadening of the spectrum line. In the present condition, the Balmer line is primarily dominated by the Stark broadening effect. Because this effect is mainly related to the existence of the electron, the electron number density could be determined from the measured spectrum. The detailed procedure for the determination will be explained later.

In the region more than 4 mm from the shock front, however, the emission from atomic nitrogen becomes dominant because all of the molecules dissociate almost completely. The typical spectrum

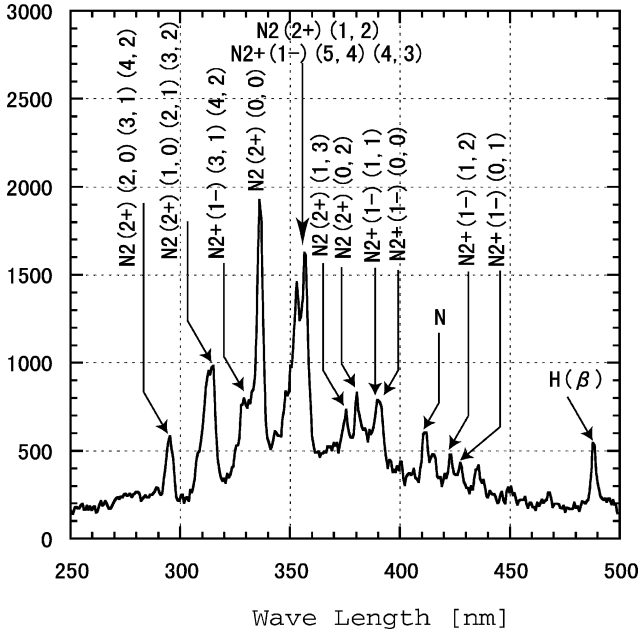

Fig. 2 Radiation spectrum at a location 1.4 mm away from the shock wave with a propagation velocity 12.4 km/s.

observed in this regime is shown in Fig. 3. As will be explained later, those emissions enable us to determine the electron excitation temperature of the atomic nitrogen by the use of the relative spectrum intensity method.

B. Spectrum in the 8 km/s Case

In the case of a shock propagation velocity of 8 km/s, it is expected that the NO molecule, which is generated just behind the shock wave, may not dissociate quickly and may even remain in the equilibrium state. This is in great contrast to the case of the shock propagation velocity of 12 km/s, where the NO molecule, once generated, dissociates very quickly. Therefore, the band tail of NO molecule, whose band head exists in the ultraviolet wavelength region (below 200 nm) affects the ultraviolet wavelength region of the molecular band spectrum of $N_2(2+)$ and $N_2^+(1-)$. In fact, because of the effect of the NO molecules, the radiation spectrum in air shows a slight difference from that of a nitrogen gas, as shown in Figs. 4a and 4b. This suggests that the contribution of not only N_2 and N_2^+, but also of NO, should be taken into account in the case of this shock propagation velocity to determine the temperatures based on the radiation spectrum behind the shock wave in air.

IV. Temperatures Distribution

A. Temperature Determination Method

1. Rotational and Vibrational Temperature Determination Method

From the measured spectrum including the band spectrum of N_2 or N_2^+, the rotational and the vibrational temperatures of the molecules could be determined. For this purpose, the spectrum fitting method was applied because the spectrum resolution obtained in this experiment is not high enough to determine the rotational temperature from the fine structure of the spectrum. For this fitting method, the theoretical prediction of the spectrum is required. For this purpose, the radiation calculation code SPRADIAN[5] was employed, which enables us to predict a radiation spectrum once the number density and temperature of each species are specified. Further details of this method are described in Refs. 2 and 6. In the case of a shock wave propagation velocity of 12 km/s, the chemical species of N_2 and N_2^+ were taken into account. In the case of the shock propagation velocity of 8 km/s, however, not only N_2 and N_2^+, but also NO, was taken into consideration for the temperature determination as mentioned in the preceding section.

The typical spectrum fitting result is shown in Fig. 5, where the shock velocity is 12.4 km/s and the spectrum was recorded at a

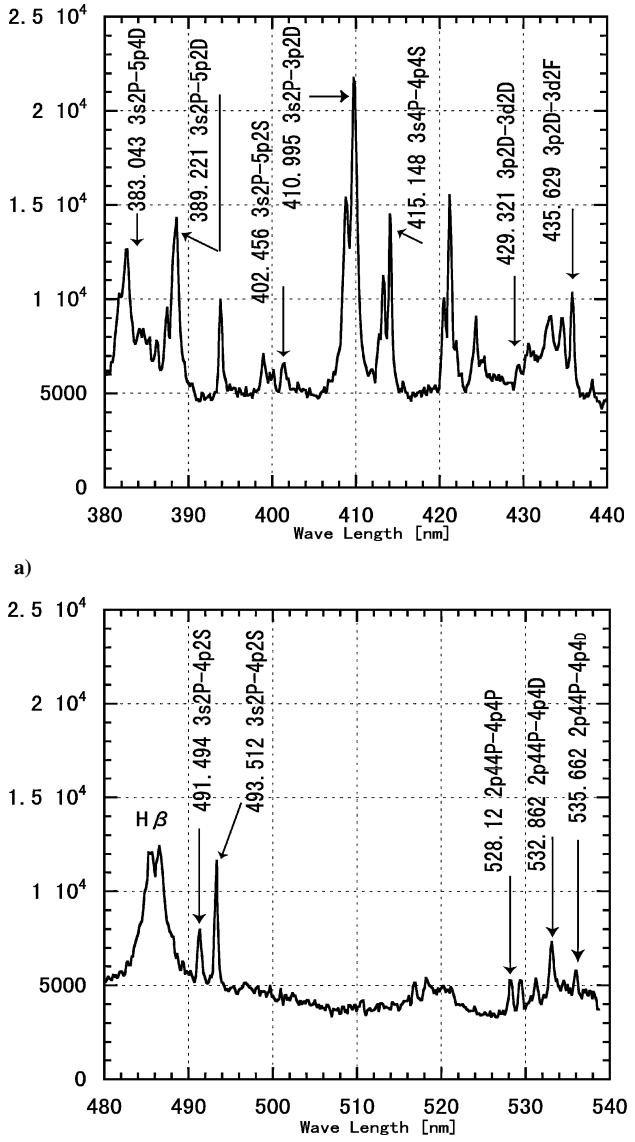

Fig. 3 Radiation spectrum of N at a location 14.87 mm apart from the shock wave with a shock propagation velocity of 12.4 km/s; the wavelength regions a) 380–440 nm and b) 480–540 nm are shown.

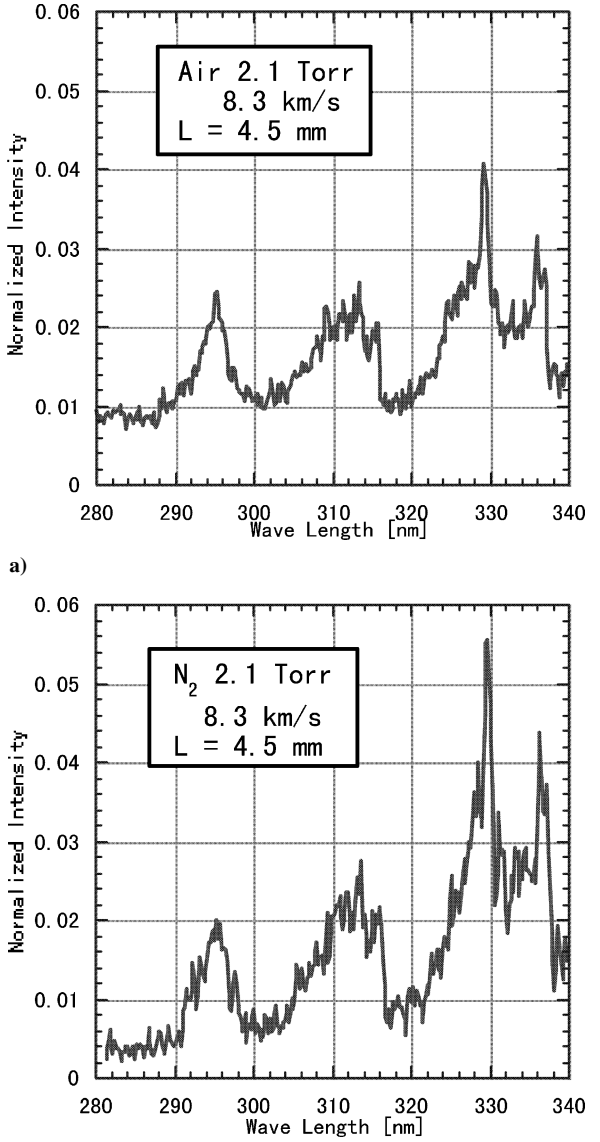

Fig. 4 Radiation spectrum a) 8.3 km/s in the case of air and b) 8.3 km/s in the case of the pure nitrogen.

location 2.3 mm away from the shock front. Both theoretical and experimental spectra agree well with each other, at least in the wavelength region shorter than 400 nm. The discrepancy observed in the wavelength region longer than 400 nm is due to the existence of the line spectra originating from the atomic nitrogen and hydrogen. From this fitting, the rotational and the vibrational temperatures of N_2 are determined to be 3500 and 5000 K, respectively, and those temperatures of N_2^+ are determined to be 17,500 and 9000 K, respectively. The spatial distribution of the temperatures can be obtained by application of this method to each spectrum measured along the distance from the shock front.

2. Electron Excitation Temperature Determination Method

From the measured spectrum that includes atomic nitrogen lines in the wavelength regions of 380–440 nm and of 480–540 nm, the electronic excitation temperature can be determined. For this purpose, the relative line intensity method[7] was applied. For the application, the correlation of the electron excitation temperature with the population of electronically excited states must be assumed. For this purpose, the Boltzmann distribution is assumed for simplicity, although the non-Boltzmann distribution model such as the quasi-steady-state model[8] may be applicable. Under this simplified assumption, the following relation appears between the radiation intensity I_{ij} and the electron excitation temperature T_{ex}:

$$\ell_n\left(\frac{I_{ij}}{g_i A_{ij}}\right) = -\frac{E_i}{k_B T_{\mathrm{ex}}} + \mathrm{const} \tag{1}$$

where k_B is the Boltzmann constant, E_i the energy level of the upper energy level, A_{ij} the transition probability from the upper ith and lower jth energy level, and g_i the statistical weight of the upper level. When the relation of Eq. (1) is fit to the measured data, the electron excitation temperature can be determined. To illustrate the procedure further, we consider the typical radiation spectra shown in Fig. 3a and 3b. In these figures, the atomic spectrum lines that were used for temperature determination are labeled with the wavelength and transition array. By the use of the transition probability A_{ij}, the statistical weight g_i, listed in Ref. 9, and the relative radiation intensity of I_{ij}, measured by the experiment, the quantity $\ell_n(I_{ij}/A_{ij}g_i)$ is plotted against the upper energy level E_i, as shown in Fig. 6. As Fig. 6 shows, the population of the electronically excited states is almost close to the Boltzmann distribution in the present energy range, which is assumed for the present temperature determination method. In this case, the electron excitation temperature was determined to be 5900 K at a distance of 14.87 mm behind the shock front.

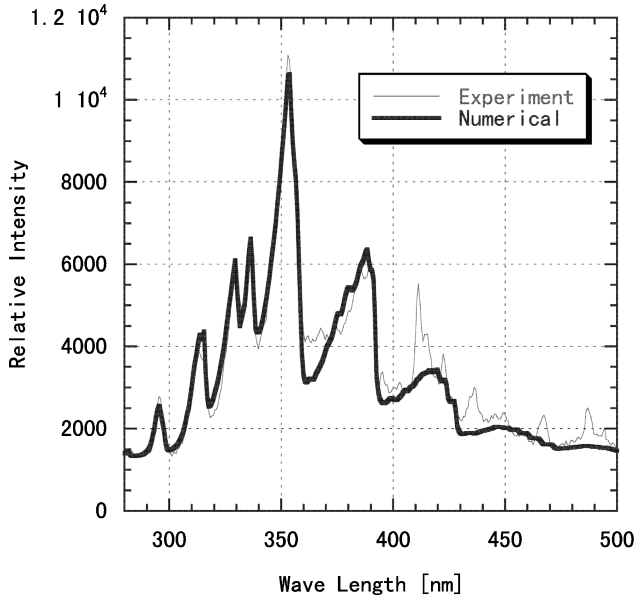

Fig. 5 Spectrum fitting results: $V_s = 12.4$ km/s and $L = 2.3$ mm for N_2 ($T_r = 3500$ K and $T_v = 5000$ K) and N_2^+ ($T_r = 17{,}500$ K and $T_v = 9000$ K).

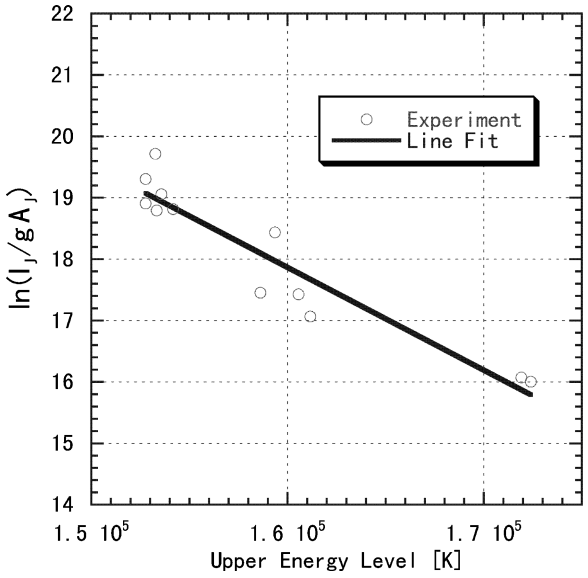

Fig. 6 Typical Boltzmann plot for the shock propagation velocity of 12.4 km/s at a distance 14.87 mm from the shock front.

B. Temperature Distribution in 8 km/s Case

In the case of a shock propagation velocity of 8.3 km/s, the temperature distributions behind the shock wave in air are depicted in Fig. 7a. In the region just behind the shock front, the measured rotational temperature is highly nonequilibrium, with the numerically predicted translational temperature. Here, the numerical prediction is based on Park's two-temperature model,[10] and it is assumed that the rotational temperature is in fully equilibrium with the translational temperature. Therefore, the nonequilibrium between them means that the rotational temperature in the experiment significantly disagrees with that in the numerical prediction, at least just behind the shock front. In the region far from the shock front, both the rotational and the vibrational temperatures are close to the equilibrium temperature, as predicted by the Park model. Even though the numerically predicted temperatures distribution is almost flat in the region, the experimentally determined temperatures increase slightly. This may be due to the effect of boundary-layer growth starting from the intersection of the shock front with the test tube wall.

Figure 7b shows an earlier result in the case of a nitrogen gas for comparison. In the case of a nitrogen gas, the discrepancy between

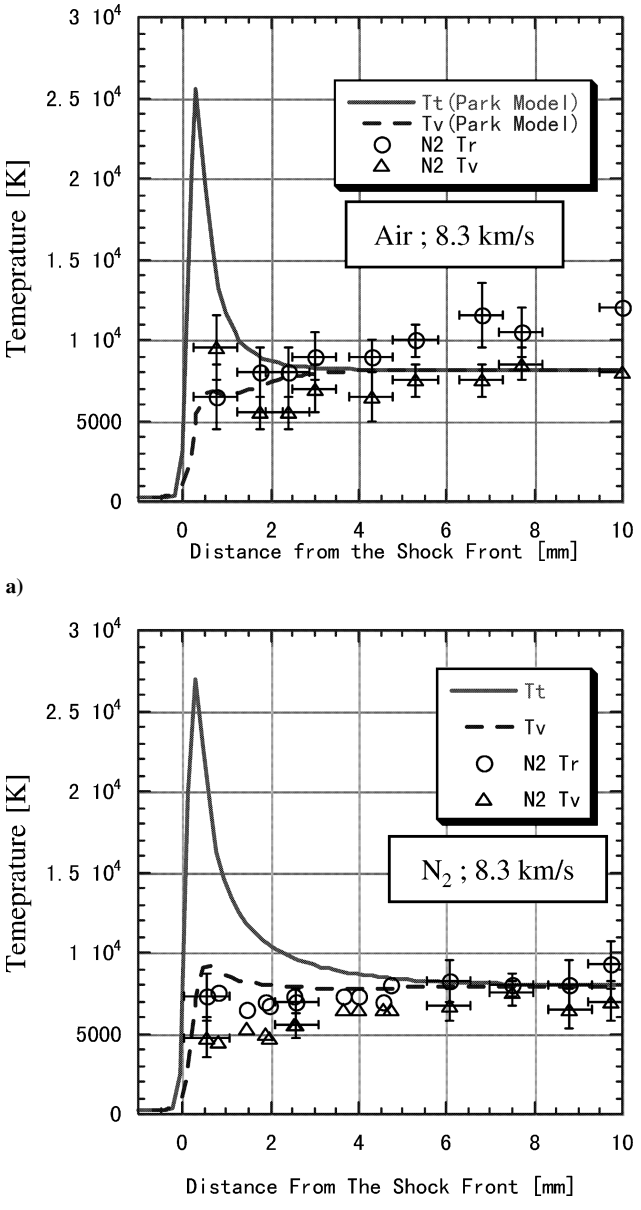

Fig. 7 Temperature distribution behind the shock wave with a propagation velocity of 8.3 km/s in the case of a) air and b) pure nitrogen gas.

the experiment and the numerical prediction in the region just behind the shock front can be also observed. Although, in the case of a nitrogen gas, the temperatures increase slightly in the region far from the shock front, it is not so obvious as that in the case of air. Such a difference between air and a nitrogen gas, however, is considered to be within the unavoidable experimental uncertainty. Therefore, the behavior of the temperatures in the case of air is concluded to be almost the same as those in the case of a nitrogen gas.

C. Temperature Distribution for 12 km/s Case

Figure 8a shows the rotational temperature distributions of N_2 and N_2^+ behind the shock wave in air in the case of 12.4 km/s. The previous result for pure nitrogen is depicted in Fig. 8b for comparison. The comparison between air and pure nitrogen will be discussed later; first of all, we will discuss the present results in air. Like the case of 8 km/s, the measured rotational temperatures disagree with the numerically predicted rotational (or translational) temperature. Again, the contradiction with the Park model is suggested.

Figure 9a shows the vibrational temperature distributions of molecules (N_2 and of N_2^+) and the electron excitation temperature distributions of atomic nitrogen in air. Note that, in the numerical

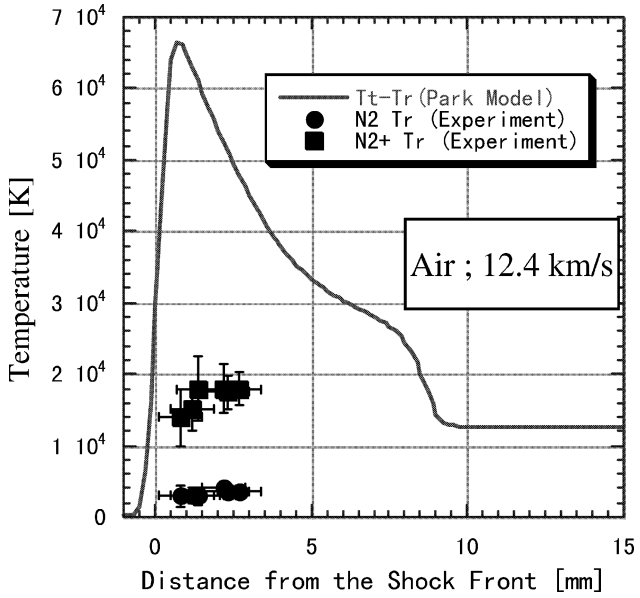

a)

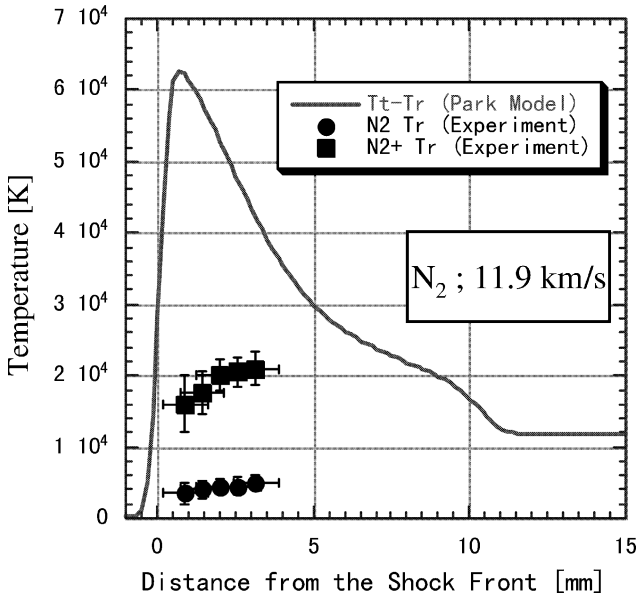

b)

Fig. 8 Rotational temperature distribution for the shock with a propagation velocity of a) 12.4 km/s in the case of air and of b) 11.9 km/s in the case of the pure nitrogen gas.

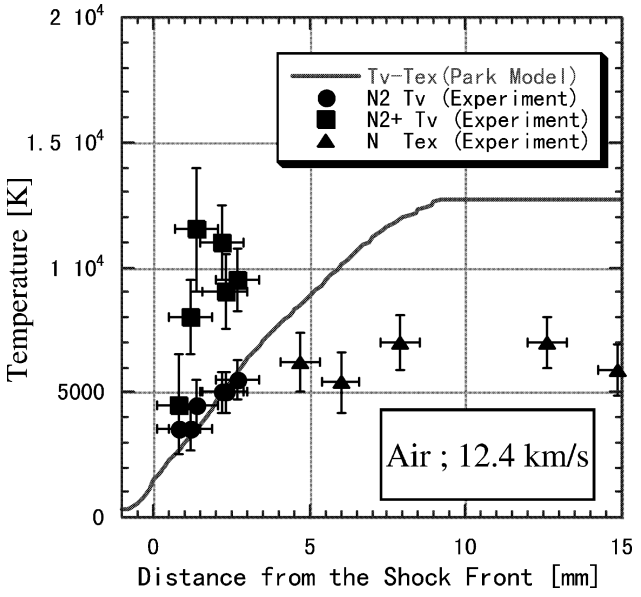

a)

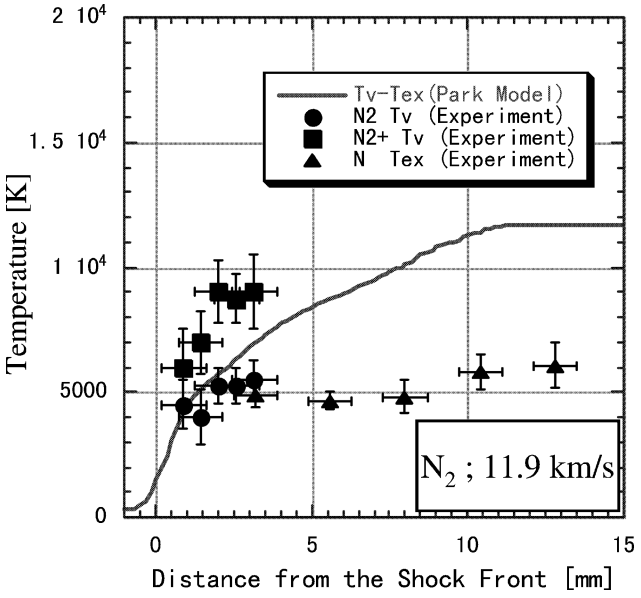

b)

Fig. 9 Vibrational and electron excitation temperature distribution for the shock with a propagation velocity of a) 12.4 km/s in the case of air and of b) 11.9 km/s in the case of a pure nitrogen gas.

prediction, the electron excitation temperature is assumed to be equilibrium with the vibrational temperature, as in the Park model. As for the vibrational temperatures of N_2 and N_2^+, their distributions are close to the numerical prediction. On the other hand, the electron excitation temperature determined by the experiment is distributed around 6000–7000 K, and is lower than that predicted by the numerical prediction based on the Park model.

The experimentally observed aerothermodynamic behavior behind the shock wave in air is summarized as follows:

1) The rotational temperatures of N_2 and N_2^+ are in nonequilibrium with the translational temperature and show the contradiction with Park's two-temperature-model.

2) The vibrational temperatures of N_2 and N_2^+ are also in nonequilibrium with the translational temperature, but almost agree with the numerical prediction.

3) The rotational and vibrational temperatures of N_2^+ are higher than those of N_2.

4) The electron excitation temperature is almost uniform and much lower than the numerical prediction.

5) The electron density distribution shows the significant disagreement with the numerical prediction in the region just behind the shock front.

Now, we will compare the present result for air with the preceding result for a nitrogen gas. In Figs. 8b and 9b, the preceding result for a nitrogen gas in the case of 11.9 km/s is shown for comparison. As Figs. 8 and 9 show, the temperature distributions observed in the experiment for air resemble that for a nitrogen gas very well. Note that the spectrum itself shows the resemblance of air to gaseous nitrogen, as shown in Figs. 10a and 10b, where the radiation spectrum observed at a distance of about 2.0 mm behind the shock front in the case of both air and nitrogen gas are shown, respectively.

Even though the difference between air and nitrogen gas is quite small in the experiment, we would likely recognize the difference in the numerical prediction for a shock velocity of 12 km/s. First of all, the distance required to reach the equilibrium state of the temperature distribution becomes considerably shorter in the case of air than it does in that of nitrogen gas, as shown in Figs. 8a, 8b, 9a, and 9b. Secondly, the vibrational temperature behind the shock wave in air increases rather slowly compared with that in a nitrogen

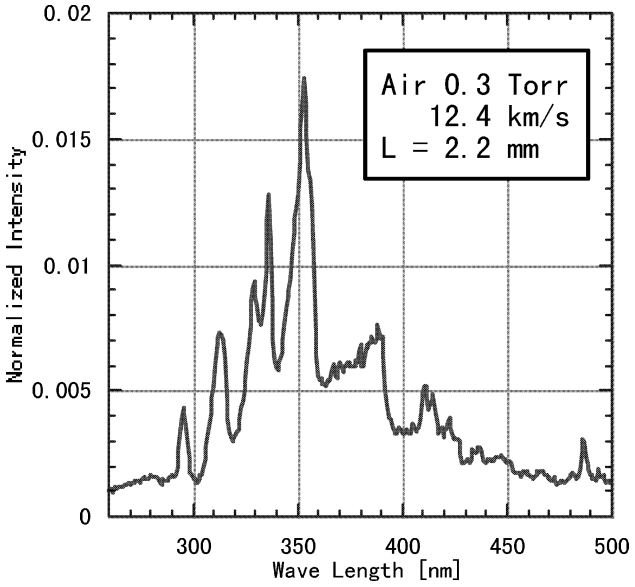

a)

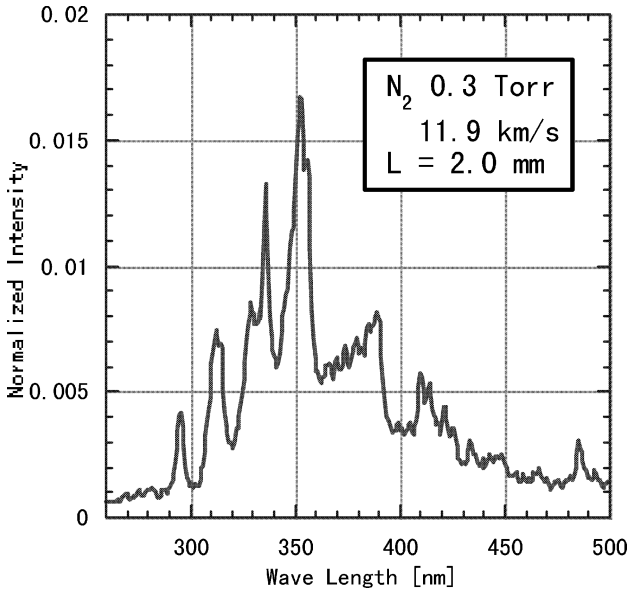

b)

Fig. 10 Radiation spectrum for the shock with a propagation velocity of a) 12.4 km/s in the case of air and of b) 11.9 km/s in the case of the pure nitrogen gas.

gas. Nevertheless it is difficult to recognize such differences experimentally. As for the distance required to reach the equilibrium state, there is no chance to recognize the difference experimentally. The reason is that, according to the numerical prediction, the region where the difference in the distance to reach the equilibrium state appears is around 10 mm behind the shock front. As mentioned earlier, no measured data are available in that region, apart from the shock front at more than 4 mm, because the molecular spectrum becomes relatively weaker due to the dissociation of the molecules, than it does due to the atomic nitrogen spectrum lines. As for the behavior of the vibrational temperature, the difference between air and nitrogen gas is, according to the numerical prediction, at most a several hundred degrees. This small difference is within the permissable uncertainty and is unavoidable in the measurement. Therefore, there are no chances to distinguish those differences experimentally.

V. Electron Density Distribution

The local electron density, compared with the electron temperature, strongly influences the Stark broadening of the Balmer line of hydrogen. Therefore, it is possible to determine the electron

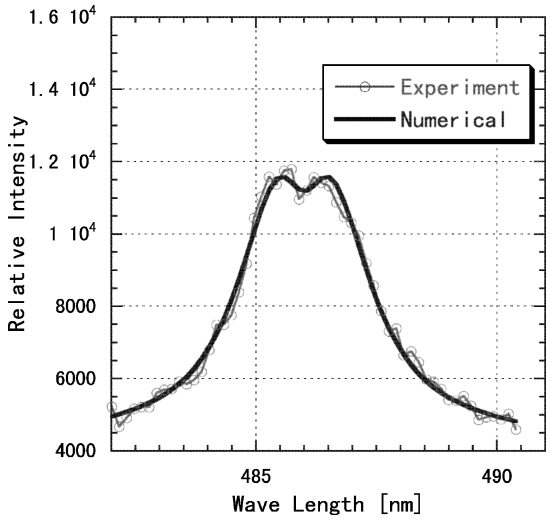

Fig. 11 Spectrum fitting for the $H\beta$ line: $V_s = 12.4$ km/s, $L = 4.85$ mm, $N_e = 4.8 \times 10^{22}$ m^{-3}, and $T_e = 30{,}000$ K.

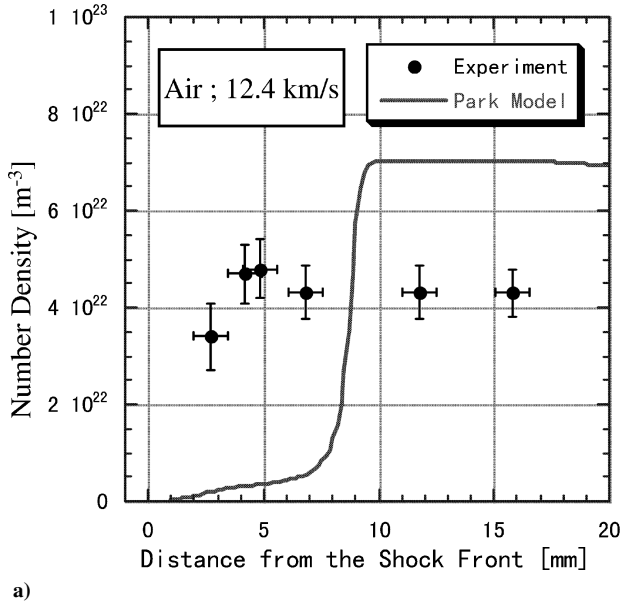

a)

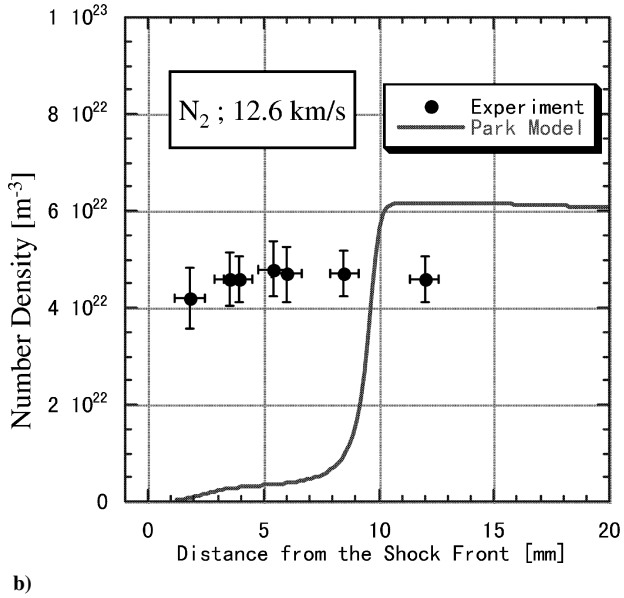

b)

Fig. 12 Electron density distribution for the shock with a propagation velocity of a) 12.4 km/s in the case of air and of b) 12.6 km/s in the case of the pure nitrogen gas.

density by application of the spectrum fitting method to the measured Balmer line. The theoretical spectrum of the Balmer line was calculated based on Ref. 11. Figure 11 shows an example of the spectrum fitting for the Balmer line. In Fig. 11, the numerical spectrum agrees with the experimental one fairly well, and it is concluded that the electron density is 4.8×10^{22} m^{-3} for the electron temperature of 3×10^4 K.

Figure 12a shows an electron density distribution determined by the application of the present method at each location behind the shock wave in air. According to the numerical prediction, the electron density increases gradually from just behind the shock wave and then, at a location approximately 7 mm behind the shock wave, it increases rapidly and reaches the equilibrium state. On the other hand, the distribution observed in the experiment is almost uniform, even in the region just behind the shock front, even though its value is fairly close to the numerically predicted electron density at the equilibrium state. That is, there is a large discrepancy between the experimental result and the numerical prediction, especially in the region just behind the shock front.

Figure 12b represents the electron density distribution in nitrogen gas for comparison. According to the numerical prediction, the electron density at the equilibrium state in air is slightly higher than in nitrogen gas, as shown in Figs. 12a and 12b. This difference, however, cannot be observed experimentally because the difference is small enough to be within the unavoidable uncertainty in the experiment. Rather, both of the experimental results hold the following common features. That is, it is expected that ionization that is much faster than that which the Park model predicts may proceed from just behind the shock front.

VI. Conclusions

The nonequilibrium aerothermodynamic behavior behind strong shock waves in air was investigated by the spectroscopic technique. It was then reviewed by comparison with earlier results for nitrogen gas to clarify the difference between air and nitrogen gas. It was found that almost similar aerothermodynamic behavior appears behind the strong shock waves. That is, no obvious effect of the oxygen-originated species appears on either the rotational and vibrational temperatures of a nitrogen-originated species such as N_2 or N_2^+, the electron excitation temperature of N, or the electron density. This is the case not only in the case of the shock propagation velocity of 12 km/s, but also in the case of a shock propagation velocity of 8 km/s, where the radiation spectrum shows a slight difference due to the effect of the NO molecule.

References

[1]Kawaguchi, J., Fujiwara, A., and Sawai, S., "Sample and Return Mission from Asteroid Nereus via Solar Electric Propulsion," *Acta Astronautica*, Vol. 38, No. 2, 1996, pp. 87–101.

[2]Fujita, K., Sato, S., Abe, T., and Ebinuma, Y., "Experimental Investigation of Air Radiation Behind a Strong Shock Wave," *Journal of Thermophysics and Heat Transfer*, Vol. 16, No. 1, 2002, pp. 77–82.

[3]Fujita, K., Sato, S., Abe, T., and Ohtsu, H., "Electron Density Measurements Behind Strong Shock Waves by H–β Profile Matching," *Journal of Thermophysics and Heat Transfer*, Vol. 17, No. 2, 2003, pp. 210–216.

[4]Ogura, E., Funabiki, K., Sato, S., and Abe, T., "Free Piston Double Diaphragm Shock Tube," Inst. of Space and Astronautical Science, ISAS Rept. 96, Kanagwa, Japan, Aug. 1997 (in Japanese).

[5]Fujita, K., and Abe, T., "SPRADIAN, Structured Package for Radiation Analysis: Theory and Application," Inst. of Space and Astronautical Science, ISAS Rept., 669, Kanagwa, Japan, Sept. 1997.

[6]Matsuda, A., Fujita, K., Sato, S., and Abe, T., "Experimental Study for the Shock Layer Generated in a Super-Orbital Reentry Flight," International Symposium on Shock Waves, ISSW Paper 1001, July 2001.

[7]Griem, H. R., *Plasma Spectroscopy*, McGraw–Hill, New York, 1964, p. 270.

[8]Park, C., "Calculation of Nonequilibrium Radiation in the Flight Regimes of Aeroassisted Orbital Transfer Vehicles," AIAA Paper 84-0306, Jan. 1984.

[9]Wiese, W. L., Fuhr, J. R., and Deters, T. M., *Journal of Physical and Chemical Reference Data*, Monograph 7, American Chemical Society and American Inst. of Physics for National Inst. of Standards and Technology, New York, 1996, p. 157.

[10]Park, C., *Nonequilibrium Hypersonic Aerothermodynamics*, Wiley, New York, 1990, pp. 326–328.

[11]Griem, H. R., Kolb, A. C., and Shen, K. Y., "Stark Broadening of Hydrogen Lines in a Plasma," *Physical Review*, Vol. 116, No. 1, 1959, pp. 4–16.